Semi Empirical Model of Global Warming Including Cosmic Forces, Greenhouse Gases, and Volcanic Eruptions

Antero Ollila[1*]

[1] *Department of Civil and Environmental Engineering (Emer.), School of Engineering, Aalto University, Espoo, Finland*
Otakaari 1, Box 11000, 00076 AALTO, Finland

1 **ABSTRACT**
2

In this paper, the author describes a semi empirical climate model (SECM) including the major forces which have impacts on the global warming namely Greenhouse Gases (GHG), the Total Solar Irradiance (TSI), the Astronomical Harmonic Resonances (AHR), and the Volcanic Eruptions (VE). The effects of GHGs have been calculated based on the spectral analysis methods. The GHG effects cannot alone explain the temperature changes starting from the Little Ice Age (LIA). The known TSI variations have a major role in explaining the warming before 1880. There are two warming periods since 1930 and the cycling AHR effects can explain these periods of 60 year intervals. The warming mechanisms of TSI and AHR include the cloudiness changes and these quantitative effects are based on empirical temperature changes. The AHR effects depend on the TSI, because their impact mechanisms are proposed to happen through cloudiness changes and TSI amplification mechanism happen in the same way. Two major volcanic eruptions, which can be detected in the global temperature data, are included. The author has reconstructed the global temperature data from 1630 to 2015 utilizing the published temperature estimates for the period 1600 – 1880, and for the period 1880 – 2015 he has used the two measurement based data sets of the 1970s together with two present data sets. The SECM explains the temperature changes from 1630 to 2015 with the standard error of 0.09 $°C$, and the coefficient of determination r^2 being 0.90. The temperature increase according to SCEM from 1880 to 2015 is 0.76 $°C$ distributed between the Sun 0.35 $°C$, the GHGs 0.28 $°C$ (CO_2 0.22 $°C$), and the AHR 0.13 $°C$. The AHR effects can explain the temperature pause of the 2000s. The scenarios of four different TSI trends from 2015 to 2100 show that the temperature decreases even if the TSI would remain at the present level.

3
4 *Keywords: Climate change, Climate model, Cosmic forces, Global warming, Greenhouse*
5 *gases*
6
7

1. INTRODUCTION

The Intergovernmental Panel on Climate Change (IPCC) has published five assessment reports (AR) about the climate change. According to IPCC the climate change is almost totally due to the concentration increases of GH gases (97.9 %) since the industrialization 1750. The Radiative Forcing (RF) value of the year 2011 corresponds the temperature increase of 1.17 ☐C, which is 37.6 % greater than the observed temperature increase 0.85 ☐C [1]. Because of the temperature pause since 2000, the error of this model is now about 49 %. This great error of the IPCC's model means that the approach of IPCC can be questioned. One obvious reason is that IPCC mission is limited to assess only human-induced climate change. In this paper, other climate changing forces Greenhouse Gases (GHG), the Total Solar Irradiance (TSI), the Astronomical Harmonic Resonances (AHR), and the Volcanic Eruptions (VE), are analyzed and their impacts on the global temperature are quantified on the theoretical and empirical ways. The objective of this paper is to construct a global temperature data set from 1610 to 2015 and to combine the above listed climate change forces on the theoretical and empirical grounds to explain the temperature changes during this period.

Table 1 includes all the symbols, abbreviations, acronyms, and definitions used repeatedly in this paper.

Table 1. List of symbols, abbreviations, and acronyms

Acronym	Definition
AGW	Anthropogenic global warming
AHR	Astronomic harmonic resonances
AR	Assessment report of IPCC
Barycenter	Gravity center of the solar system
CF	Cloud forcing
CS	Climate sensitivity
CSP	Climate sensitivity parameter (=λ)
ECS	Equilibrium climate sensitivity
GCR	Galactic cosmic rays
GH	Greenhouse
GHG	GH gas
GISS	Goddard Institute for Space Studies
HadCRUT4	Temperature data set of Hadley Centre
IPCC	The Intergovernmental Panel on Climate Change
ISCCP	International Satellite Cloud Climatology Project
LIA	Little ice age
NH	Northern hemisphere
RF	Radiative forcing change
SECM	Semi empirical climate model
SH	Southern hemisphere
TCS	Transient climate sensitivity
T-est	Proxy temperature estimate
T-rec	Measured temperature
T-comp	T-est + T-rec
UAH	University of Alabama in Huntsville
VE	Volcanic eruptions

2. CONSTRUCTION OF THE GLOBAL TEMPERATURE FROM 1610 TO 2015

2.1 Estimated global temperature from 1610 to 1890

There is no generally accepted temperature data for the period from 1610 to 1890 because there have been no global temperature recording methods available. Therefore, all the global temperatures for this period are estimated using different proxy methods. The author has selected three commonly used proxy data sets namely Briffa et al. [2] applying tree ring density data, Moberg et al. [3] applying tree ring data and lake and ocean sediment data, and Ljungqvist [4] applying nine different proxy methods. The data sets are normalized to give zero Celsius degrees for the period from 1877 to 1883, because the year 1880 is generally used as a starting point for the recorded temperatures. The three data sets and the average data set is depicted in Fig. 1.
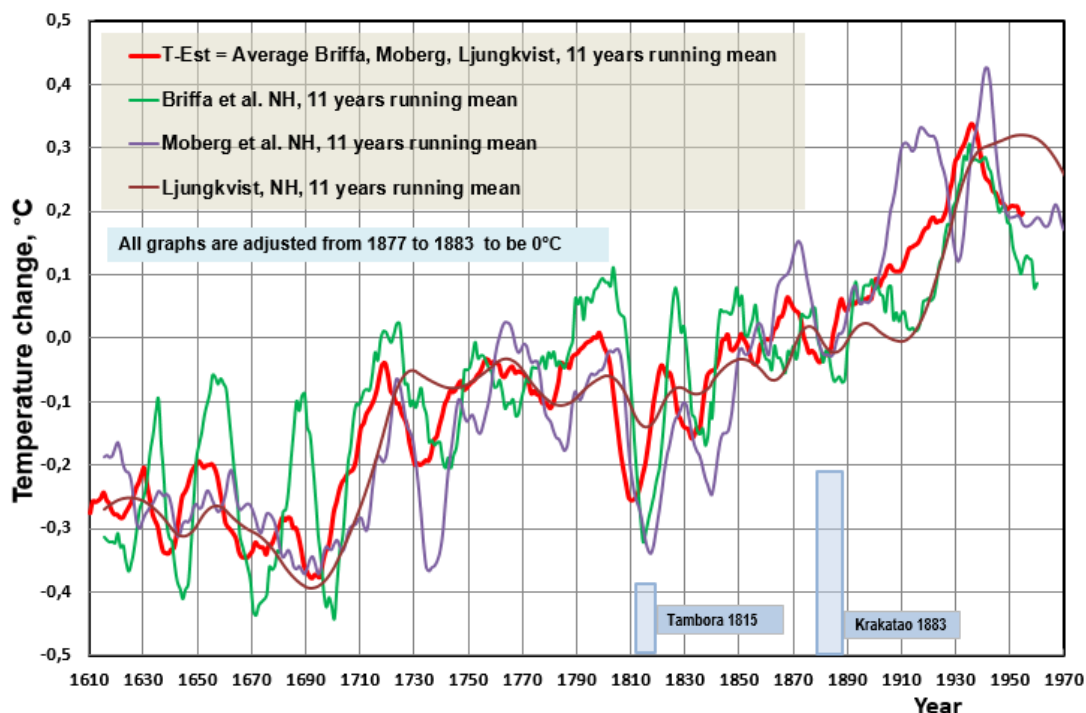
Figure 1. Estimated global temperature T-Est constructed as the average of three temperature proxies.

All three temperature graphs show the same kind of overall trend from 1610 to 1890. The temperature decrease caused by the Tambora eruption in 1815 can clearly be seen but the Krakatoa temperature decrease is significantly smaller. It appears that the graph of Briffa et al. [2] is the most sensitive for temperature changes. It is natural that the graph of Ljungqvist [4] is the most insensitive in regard to changes because the averaging of the nine different proxies smoothens out the changes. The arithmetical average of these three different proxy temperatures may be a good compromise regarding sensitivity for temperature changes.

The three data sets applied cover the northern hemisphere (NH) only. The NH and SH satellite data sets of the University of Arizona in Huntsville (UAH) [5] shows that the difference of the average values from 1980 to 2015 is only 0.013 □C. This small difference means that it is justified to use NH temperatures as the global temperature change as well.

62
63 **2.2 Recorded global temperature from 1880 to 2015**
64
65 HadCrut4 [6] temperature data set starts from 1850 but the coverage of the data is not very
66 good. A special problem has been detected in different data set versions of GISS [7]. The
67 versions of the year 2000 and 2016 of this data and the satellite temperature data set of
68 UAH are depicted in Fig. 2.
69
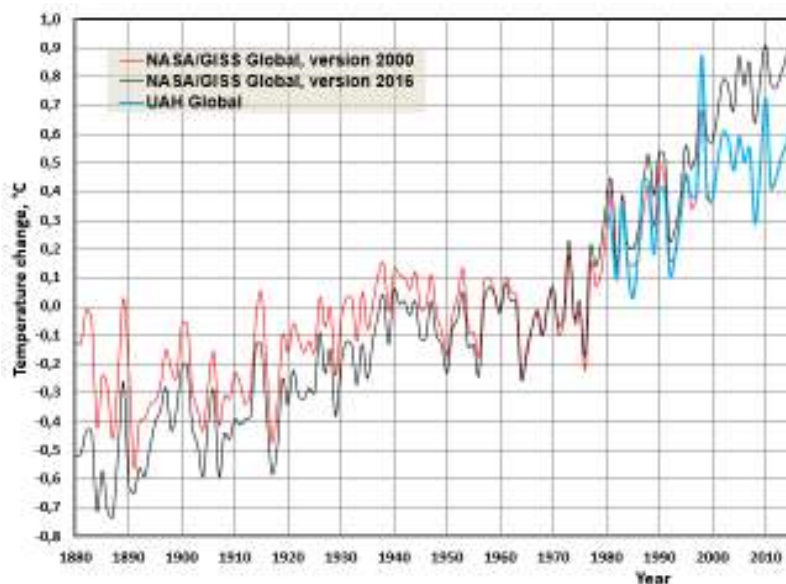
70
71 **Figure 2. The temperature data versions 2000 and 2016 of NASA/GISS [7] and UAH [5].**
72
73 The temperature increase from 1880 to 2000 has been 0.47 □C according to GISS version
74 2000, and the increase for the same period has been 1.09 □C according to version 2016. As
75 one can see in Fig. 2, the version 2016 (GISS-16) temperature in 1880 has been much lower
76 but the temperature in 2000 is higher than the one of the version 2000. Also, the average
77 temperature of GISS-16 [7] during the period from 2000 to 2015 is 0.26 □C higher than that
78 of UAH [5]. These new versions have been adjusted in the name of data homogenization.
79 Another suspicious element in the GISS data sets is the warming during 1930s. The extreme
80 weather events like heat waves and draughts in USA [8, 9] related to high temperatures
81 show that in 1930s these events have been stronger and more frequent than during the
82 2000s. Therefore, the author has been looking for older data before 1979, which was the
83 starting year of UAH temperature data set.
84
85 In 1974, the Governing Board of the National Research Council of USA established a
86 Committee for the Global Atmospheric Research Program. This committee consisted of tens
87 of the front-line climate scientists in USA and their major concern was to understand in which
88 way the changes in climate could affect human activities and even life itself. A stimulus for
89 this special activity was not the increasing global temperature but the rapid temperature
90 decrease since 1940. There was a common threat of a new ice age. The committee
91 published in behalf of National Academy of Sciences the report [10] by name "Understanding
92 Climate Change – A Program for Action" in 1975. The committee had used the temperature
93 data published by Budyko [11], which shows the temperature peak of 1930s and cooling to
94 1969. This digitized temperature graph from 1880 to 1969 is depicted in Fig. 3. The
95 temperature peak of 30s is little bit lower in the graph published by Hansen [12]. There is
96 another global data graph published by Angell and Korshover [13] from 1957 to 1975

97 following the trend of Byduko [11] but because it so short a period, it has not been used. In
98 constructing the recorded global temperature data set T-rec, the author has used the
99 average of Budyko [11] and Hansen [12] data from 1880 to 1969. The temperature change
100 from 1969 to 1979 is covered by the GISS-16 data and thereafter by UAH [5]. The UAH data
101 has been normalized to GISS-16 [7] by equaling the average values from 1979 to 1981. All
102 these data set values are depicted in Fig. 3.
103
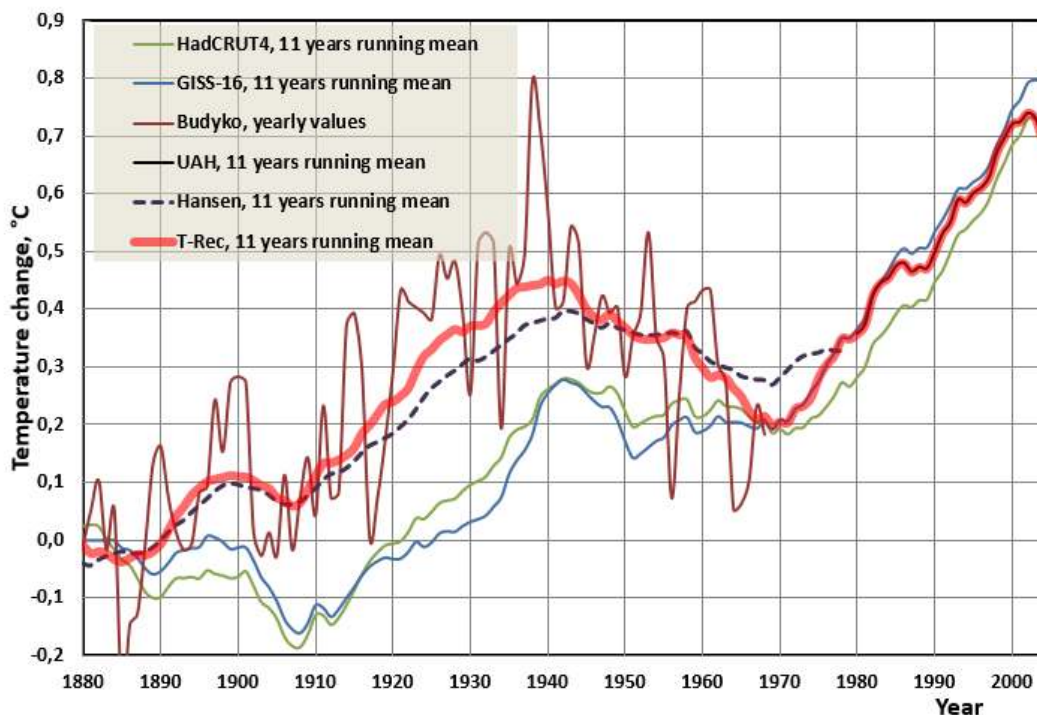
104
105 **Figure 3. The different recorded temperature data set and the constructed data set T-**
106 **rec.**
107
108 The constructed data set T-rec is normalized by averaging the decade 1880 to be same as
109 that of T-est. The constructed T-rec shows the peak value of 1930s to be about 0.25 □C
110 lower than the 2000s. The same difference in the GISS-00 (version 2000) is about 0.3 □C
111 and in the GISS-16 version the difference is about 0.6 □C. As references, there are GISS-16
112 [7] and HadCrut4 [6] temperature graphs also depicted in Fig. 3. The difference between
113 these data sets and T-rec is even 0.35 □C during the period from 1880 to 1950. In the late
114 1970s the differences between different data sets are almost neglectable, when the present
115 warming was in the early phase. A general conclusion is that the history (1880-1960) of the
116 global temperature of the new versions of GISS is getting colder and the newer
117 temperatures of 2000s are getting warmer. These changes, which happen always in the
118 newer versions of GISS, arouse doubts of justification of these changes. Soon et al. [14]
119 have analyzed that the rural land-based meteorological stations data results into a
120 temperature trend, which deviate from the official temperature trends especially during 30s, it
121 is very close to T-rec calculated in this study. Their conclusion is that the urban heat island
122 syndrome of meteorological stations has caused a bias into the measurement data.
123 Therefore, the author considers that the T-rec constructed from the older global temperature
124 data sets is more reliable than the GISS [5] and HadCRUT4 [7] temperature data. The
125 combination of the T-est and T-rec is labelled as T-comp, which is valid from 1630-2015.
126

3. DEVELOPMENT OF SEMI EMPIRICAL CLIMATE MODEL (SECM)

3.1 Temperature impacts of greenhouse gases (GHG)

According to IPCC[1] the climate change is almost totally due to the concentration increases of GH gases since the industrialization 1750 and the global warming can be calculated using Eq. (1) [15]:

$$dT = CSP * RF \tag{1}$$

where dT is the temperature change (K) since 1750, CSP (also marked by λ) is a climate sensitivity parameter ($K/Wm^{-2)}$) and RF is radiative forcing (Wm^{-2}) caused by GH gases and other drivers. The total RF in AR5 [15] was 2.34 Wm^{-2} in 2011 and the RF value of solar irradiance was 0.05 Wm^{-2}, which means 2.1 % positive contribution. The CSP is nearly invariant <mark>parameter according to IPCC [15] having</mark> a typical value about 0.5 $K/(Wm^{-2})$.

The transient climate sensitivity (TRC) according to Eq. (1) and the RF value of 3.7 Wm^{-2} for CO_2 is 1.85 □C [16] and it is close to the average TRC 1.75 □C (from 1.0 □C to 2.5 □C) reported in the AR5 [1]. The equilibrium climate sensitivity (ECS) reported in AR5 [1] is in the range 1.5 □C to 4.5 □C, which means the average ECS to be 3.0 □C. Several researchers have reported much lower ECS values than 3.0 □C (the best estimates / the minimum values): Aldrin [17] 2.0 □C / 1.1 □C; Bengtson & Schwartz [18] 2.0 □C / 1.15 □C; Otto et al. [19] 2.0 □C / 1.2, and Lewis [20] 1.6 □C / 1.2 □C. In the above referred studies the RF [16] value of 3.7 Wm^{-2} for CO_2 has been used. It means that the CSP values of these studies are essentially lower than 0.5 K/Wm^{-2} and it means that there is no positive water feedback. Harde [21] has used spectral analysis methods and the two-layer climate model in calculating the ECS values and his result is 0.6 □C. Ollila [22] has also reported the ECS value of 0.6 □C by utilizing spectral analysis and no water feedback in CSP and in RF formula:

$$dT = 0.27 \ K/(Wm^{-2}) * 3.12 * \ln (CO_2/280) \tag{2}$$

where CO_2 is the actual CO_2 concentration (ppm). The warming effect of CO_2 according to Eq. (2) until to 2015 is 0.28 □C. Ollila [23] has shown that the total precipitable water (TPW) changes are neglectable from 1979 to 2015 challenging the assumption of the constant relative humidity assumption of IPCC. Ollila [24] has combined the warming effects of CH_4 and N_2O into one linear equation based on the spectral analysis calculations:

$$dT = -0.5558 + 0.0003176 * Year \tag{3}$$

The temperature increase by CH_4 and N_2O from 1750 to 2015 is 0.083 □C according to Eq. (3).

3.2 Temperature impacts of total solar irradiance (TSI) changes

The second element in the SECM is TSI (Total Solar Irradiance) changes caused by activity variations of the Sun. The TSI changes have been estimated by applying different proxy methods. Lean [25] has used sunspot darkening and facular brightening data. Hoyt and Schatten [26] have used three different indices namely sunspot structure, solar cycle, and equatorial solar rotation rate data. Bard [27] has used isotopes ^{14}C and [10]Be production rates in evaluating the solar magnetic variability. These TSI trends based on these three methods are depicted in Fig. 4. There are similarities and differences between these three trends.
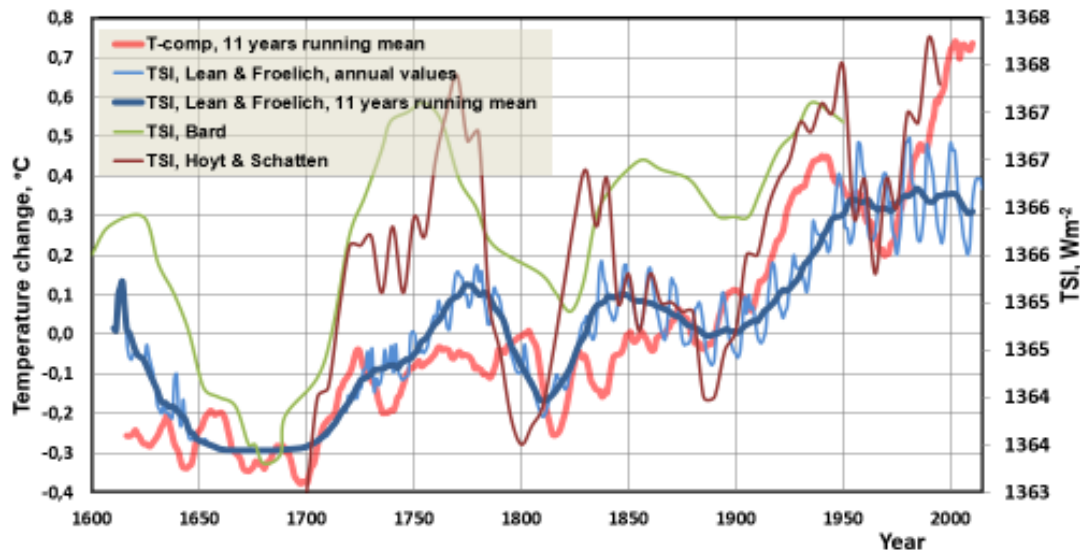
Figure 4. TSI from 1610 to 2014 Lean [25], PMOD [28], Bard [27] and Hoyt & Schotten [26] and the global temperature T-Comp.

The author has selected the data set of Lean [25], which is available to 2000 and combined this data to the data of PMOD data set [28] from 2000 onward. According to this data, TSI has increased 2.75 Wm^{-2} since the 1650's as depicted in Fig. 4. The direct warming impact can be calculated by Eq. (4) derived from the Earth's energy balance

$$T = (TSI*(1-\alpha)/4s))^{0.25} \qquad (4)$$

where α is the Earth's total albedo, and s is Stefan-Bolzmann constant. The dependency of the Earth's albedo on the cloudiness can be calculated based on the three pairs of cloudiness and albedo values [29]. Cloudiness-% values are 0 %, 66 %, and 100%. The cloudiness-% of 66 is the average all-sky value of the present climate. The corresponding albedo values can be calculated according to the albedo specification by dividing the total reflected shortwave radiation flux by the total solar radiation flux (324 Wm^{-2}): 53/342, 104.2/342, and 120/342). These three pairs of data are fitted to the second order polynomial:

$$\alpha = 0.15497 + 0.0028623 * \text{cloudiness-\%} - 0.000009 * (\text{cloudiness-\%})^2 \qquad (5)$$

McIntyre & McKitrick [30], Alley [31], Ljungvist [4], and Esper et al. [32] have come into conclusion that there have been at least two warm periods about 1000 and 2000 years ago. The direct irradiance changes have not been big enough to explain these changes, because the direct temperature impact by TSI change from 1650 to 2015 is 0.12 □C. In the pioneer research Svensmark [33] has introduced evidence about the phenomena in which solar cycle variations modulate galactic cosmic ray (GCR) fluxes in the earth's atmosphere, which phenomenon could cause clouds to form. They argued that cosmic ray particles collide with particles in atmosphere, inducing electrical charges on them and nucleating clouds. Svensmark et al. [34] have found further evidences about this mechanism by studying the coronal mass ejections from the Sun. They found that low clouds contain less liquid water following cosmic ray decreases caused by the Sun. This mechanism amplifies the impacts of the original changes in the Sun's activity on the Earth's climate but the researchers have not been able to calculate the quantitative effects of TSI changes.

The author has calculated the empirical warming effects of TSI changes on the three

periods: 1665 – 1703, 1844 – 1873, and 1987-1991. The periods are selected so that the positive and negative temperature effects of Astronomic Harmonic Resonances (AHR) during these periods compensate each other, see section 4. The first period acts as a reference period, when the warming impacts of the Sun are zero. The observed temperature changes caused by the TSI changes during the two other periods are calculated by subtracting the dT caused by the GH gases from the observed dT-comp. The cloudiness-% of the selected periods are calculated applying Eq. (4) and Eq. (5). The cloudiness-% of 1987-1991 is practically same as the one from the ISCCP data set [35].

Table 2. TSI, albedo, cloudiness, and temperature changes during three periods.

Period	TSI, Wm^{-2}	dT, $°C$	Albedo	Cloudiness-%
1665-1703	1363.45	0.0	0.308807	68.5
1844-1873	1365	0.24	0.306988	67.4
1987-1991	1366.2	0.50	0.304343	66.0

The relationship between the temperature change and the cloudiness-% change can be fitted by the 2. order polynomial, which is slightly nonlinear:

$$dT = -457777.75 + 671.93304 * TSI – 0,2465316 * TSI^2 \qquad (6)$$

where dT ($°C$) is the temperature change by the TSI. During the analyzed period from 1630-2015 the corresponding albedo and temperature changes are calculated by Eq. (4) and Eq. (5). The temperature change of 0.50 $°C$ caused by TSI change of 2.67 Wm^{-2} can be divided between the direct impact of TSI change 0.12 $°C$ and the cloudiness-% decrease of 2.67 % causing the temperature increase of 0.38 $°C$. Cloud forcing according to Eq. (4) and Eq. (5) is 1.7 $°C$/cloudiness-% and this relationship is inc luded in Eq. (6). In this analysis, the cloudiness-% decrease from 68.5 to 66 explains the amplification of TSI increase. Because we do not have real cloudiness measurements before 1980, we do not know exactly what have been the real cloudiness variations before that year. Kauppinen et al. [36] and Ollila [29] have reported that the cloudiness forcing is -0.1 °C/cloudiness-% using two different approaches. According to this cloud forcing, the cloudiness-% change needed to explain the temperature change would be from 69.45 to 66.0. Anyway, the empirical result is that the relatively small cloudiness changes can explain, why the temperature effect of the TSI changes are amplified by a factor = 0.5 $°C$ / 0.12 $°C$ = 4.2.

3.3 Temperature impacts of astronomical harmonic resonances (AHR)

The third element of the SECM is a phenomenon called Astronomical Harmonic Resonances (AHR). This approach has proposed Scafetta [37]. He found that large climate oscillations with peak-to-trough amplitude of about 0.1 $°C$ and 0.25 $°C$, and periods of about 20 and 60 years, respectively, are synchronized to the orbital periods of Jupiter (29.4 years) and Saturn (11.87) years.

Ermakov et al. [38] have proposed that the influence mechanism of the AHR happens through the variations of space dust entering the Earth's atmosphere. The estimates of daily dust amount vary from 400 to 10 000 tons. The optical measurement of the Infrared Astronomical Satellite (IRAS) revealed in 1983 that the Earth is embedded in a circumsolar toroid ring of dust [39], Fig. 5. This dust ring co-rotates around the Sun with Earth and it locates from 0.8 AU to 1.3 AU from the Sun [40].
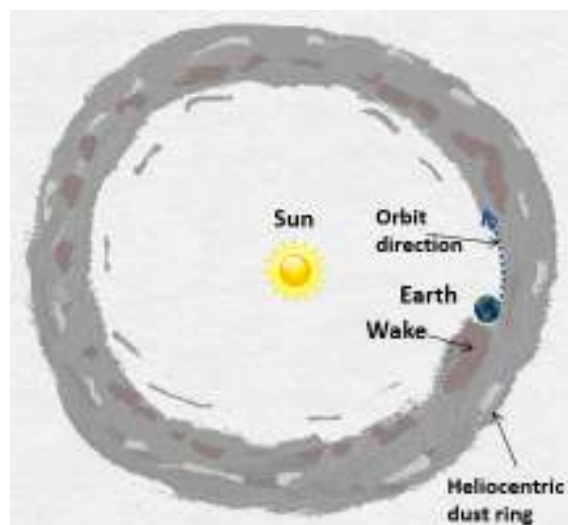
263
264 **Figure 5. A schematic picture of the circumsolar dust cloud reproduced by the author**
265 **according to the presentation of the numerical simulations [40].**

266
267 In the wake of the Earth is the permanent trail of dust particles having about 10 % greater
268 density than the background zodiacal cloud. The darker spots in Fig. 5 represent higher
269 concentrations of dust. Gold [39] has pointed out that the small particles in the Solar System
270 spiral toward the Sun but they may become trapped in resonances with the planets. This
271 should result the circumsolar dust cloud, which is not uniform. Dermott et al. [41] have shown
272 by numerical simulations that the trailing density of the cloud is higher than the leading
273 density and this is confirmed by the IRAS quantitative measurements. Simulations show that
274 the dust particles are trapped in a 5:6 resonance with the Earth with the results that their
275 paths are not symmetric about the Sun-Earth line. According to Dermott et al. [41] this
276 asymmetric nature of the heliocentric dust cloud leads to greater dust amount encountering
277 the Earth during September-October when the Earth is closest to the trailing cloud.

278
279 Variations in dust amounts happen during a longer time scale depending on the periodicities
280 of the planets, which can move the dust cloud position in the Earth's orbit. Scafetta [37] has
281 proposed that the climate can also be directly influenced by the magnetic field oscillations
282 caused by the perturbations of the planets. AHR resonance, collective synchronization and
283 feedback mechanisms could amplify the effects of a weak external periodic forcing. In the
284 same way that galactic cosmic rays (GCR) cause ionization in the atmosphere, dust particles
285 can do the same phenomenon. In this respect, the cosmic ray model and the cosmic dust
286 model have a common meeting point but the original reasons are different: The Sun activity
287 changes and planetary periodical motions as illustrated in Fig. 6.

288
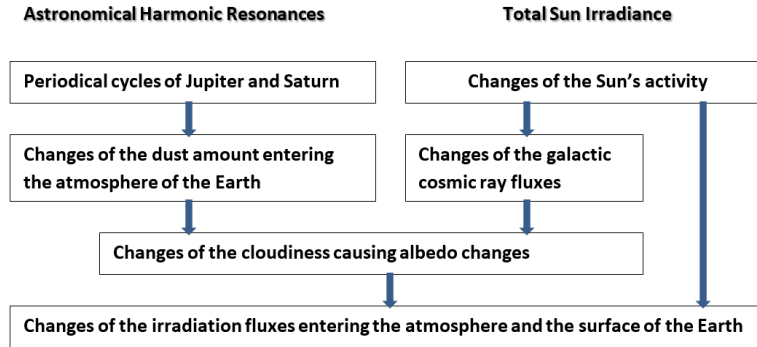
Figure 6. The influence mechanisms of TSI changes and Astronomic Harmonic Resonances (AHR).

Ollila [24] has analyzed that using the graphical data of Ermakov et al. [38] and the GH gas warming effects, the correlation between the combined model (AHR, TSI and GH gases) and the real temperature data is very good with the coefficient of correlation r^2 being 0.957 from 1880 to 2015. The calculated correlation in this case is not based on the quantified warming effects of AHR and TSI. The major objective of this paper is to assess the quantified effects AHR and TSI changes on the global temperature starting from the LIA. The periodicities caused by Jupiter and Saturn can be found in the calculated speed variations of the Sun around the Solar System Barycenter (SSB). The author has used the Horizon's application of NASA [42] in depicting the graphs in Fig. 7.
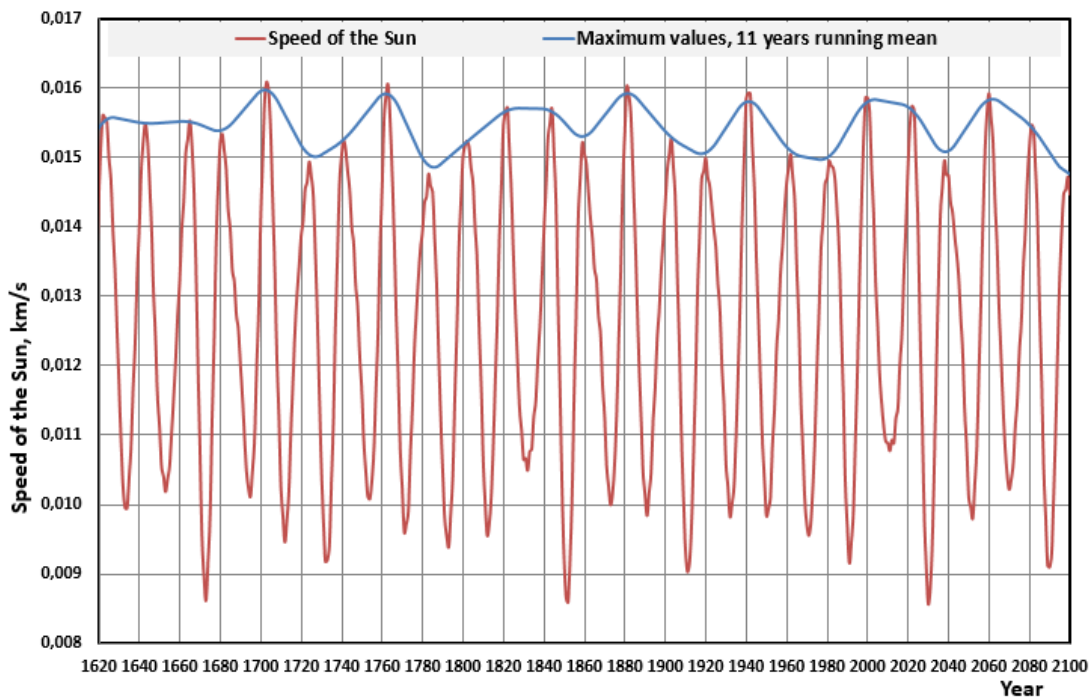
Figure 7. The speed variations of the Sun around the Solar System Barycenter.

In Fig. 7 is also depicted the variations of the maximum speed values (blue line) of the 20 years' cycles. This graphical line is 11 years running average. It should be noticed that the speed variations are not fully symmetric around the average speed and thus the temperature effects are also asymmetric. The 60-year's cycle can be easily detected. These temperature

310 effects of the AHR changes are based on the speed changes of the Sun. The magnitude of
311 the AHR effect is calculated on the empirical basis. The change from 1941 peak temperature
312 +0.185 □C to the minimum temperature -0.15 □C in 1962 is used to estimate the AHR
313 impact:

315 $dT = -6.43125 + 418.75 * SS$ (7)

317 where dT (□C) is the temperature change and SS is the Sun speed (kms^{-1}).

319 Because the TSI variations and the AHR variations finally happen through the cloudiness
320 changes, these effects cannot be summarized directly. The average cloudiness-% according
321 to ISCCP [35] is about 66 % and the average cloud layer is from 1.6 km to 4.0 km [43].
322 When the low activity of the Sun has increased cloudiness to its maximum value, the
323 cloudiness growth by nucleation process increase cannot increase the cloudiness anymore.
324 It means that 1) the humidity in the atmosphere is not adequate to increase the cloudiness
325 area over the drier areas of the globe even though the nucleation process has increased or
326 2) the AHR actually changes the thickness and the mass of the existing clouds but these
327 changes do not change the area of the clouds. When the Sun's activity is in maximum, the
328 cloudiness changes by AHR can have a full effect, because in these conditions the
329 nucleation process controls the amount of cloudiness. In calculating this relationship, the
330 author has used a factor, which has a sinusoidal dependency on the TSI value: TSI of
331 1363.43 Wm^{-2} during the LIA gives factor value zero and the TSI value of 1366.2 Wm^{-2}
332 during the present maximum gives the value = 1. The sinusoidal dependency smoothens the
333 changes close to the maximum and the minimum TSI fluxes.

3.4 Temperature impacts of major volcanic eruptions (VE)

337 The strong volcanic eruptions, which have the Volcanic Explosivity Index (VEI) 5 or 6, have
338 capacity to create eruption columns reaching the stratosphere [44]. The best documented
339 eruption of this kind was the Mt. Pinatubo eruption in 1991. The aerosol cloud covered the
340 latitudes from 60S to 60N after three months and in six months the cloud was uniform over
341 the hemispheres [45]. These kinds of eruptions typically reduce the global temperature by
342 0.5 □C from 2 to 5 years. During the period from 1600 to 2015 there has been four volcanic
343 eruptions with VEI index 5-7 namely Tambora 1815, Krakatoa 1883, Novarupta 1912, and
344 Pinatubo 1991. In the global temperature record constructed in this research, the eruptions
345 of Tambora and Krakatoa can be identified but the Novarupta ja Pinatubo effects disappear
346 in the 11 years running mean presentation. The temperature effects of both eruptions have
347 been estimated in the same way. The temperature decrease starting from the eruption year
348 and the consecutive years have been -0.5 □C, -0.35 □C, -0.1 □C, and -0.05 □C.

3.5 The summary of the SECM temperature effects

352 The estimated and observed temperature T-comp and the temperature by the SECM are
353 depicted in Fig. 8. All temperatures are smoothed by 11 years running average. The average
354 values of the SECM and T-comp are normalized to be the same for the period from 1630 to
355 2015. This figure shows that the global temperature does not follow the monotonically
356 increasing temperature effect of GH gases. The major driver of the climate change is the
357 Sun. The AHR explain the strong temperature peaks of 30's and the now in 2000's. Without
358 the AHR effects the total explanation power of SECM would be much weaker since 1900.
359 Because the temperature effects depend on the Sun activity, the magnitude of AHR effects
360 disappears totally in 1600s. The coefficient of correlation r^2 = 0.90 for the period from 1630
361 to 2015 and the standard error of estimate is 0.09 □C.
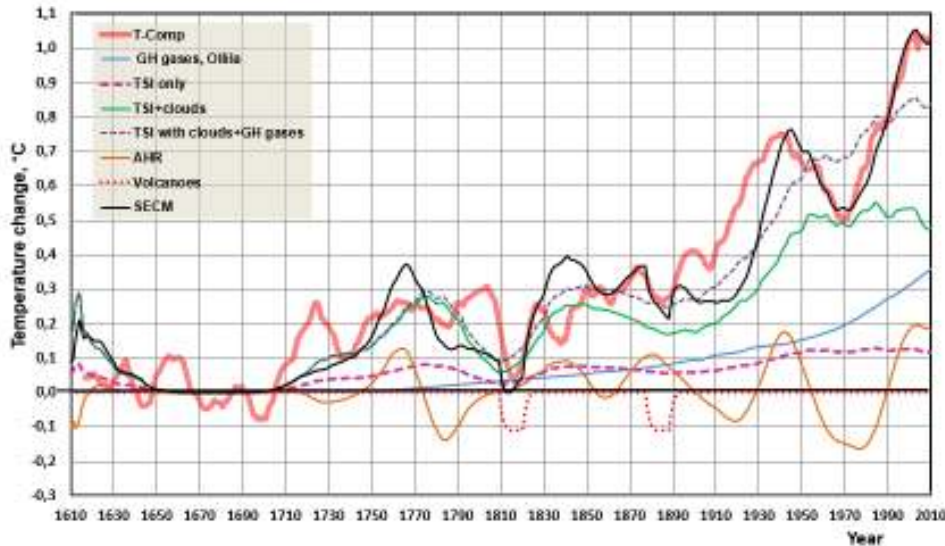
Figure 8. The estimated and observed temperature T-comp and the temperature by SECM. All temperatures are smoothed by 11 years running <mark>mean</mark>.

The average contributions of the different climate forcing elements during the centuries and in year 2015 have been summarized in Table 3.

Table 3. The summary of warming effects during the centuries, %.

Century	Sun	GHGs	AHR	Volcanoes
1700-1800	99.5	4.6	-4.0	0.0
1800-1900	70.6	21.5	17.4	-9.4
1900-2000	72.5	30.4	-2.9	0.0
2015	46.2	37.3	16.6	0.0

The Sun's contribution is the greatest but the warming effect of GHGs is steadily increasing having the impact of 37.3 % in 2015. The average contribution of AHRs is zero in the long run but during the shorter periods they may be positive or negative.

3.6 The future temperature scenarios by the SECM

The possible scenarios depending on the future changes in the Sun's activity can be easily calculated using the SECM. The author has selected four different scenarios with different decreasing TSI trends in 35 years: Scenario 1, TSI decrease $-3Wm^{-2}$; scenario 2, TSI decrease -2 Wm^{-2}; scenario 3, TSI decrease -1 Wm^{-2}; scenario 4, TSI decrease 0 Wm^{-2}. After the decrease phase, the TSI flux stays at the same level to 2100. These scenarios are depicted in Fig. 9.
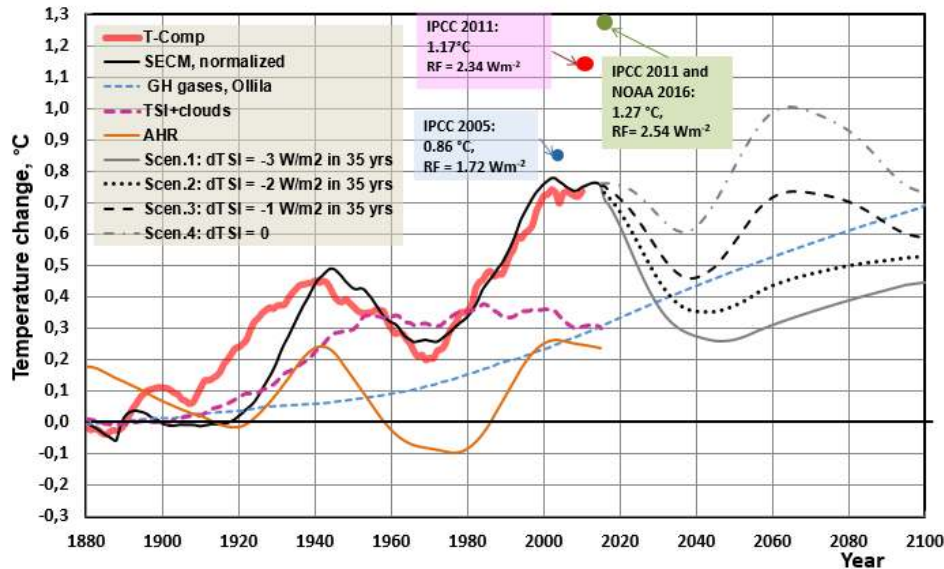
Figure 9. Four scenarios from 2015 to 2100 using four different TSI change trends.

The behavior of the Sun has been difficult to predict for researchers. The two dynamos model of the Sun developed by Shepherd et al. [46] explains very well the Sun's activity during the last three solar cycles. This model predicts that the Sun's activity approaches the conditions, where the Sun spots disappear almost totally during the next two solar cycles like during the Maunder minimum. The AHR effect explains, why the present temperature pause has continued so long, because the positive peak duration is exceptionally long, Fig. 7. Because the AHR effect also turn to a decreasing phase after 2020, the temperature would start to gradually decrease regardless of the Sun's activity change trend.   In Fig. 9 the temperatures according to the IPCC model are depicted for the years 2005, 2011 and 2016. The error in comparison to the observed temperature is very clear and if the temperature does not increase in the coming years, the error is becoming intolerable.

4. DISCUSSION

The constructed average global temperature T-comp is a combination of the average of the three historical proxy data sets from 1610 to 1890 and the combination of observed temperature data sets from 1889 to 2015. The correctness and accuracy is difficult to estimate, because the measurement based data sets deviate from each other up to 0.3 ☐C in yearly values. The three selected temperature proxy graphs show the same kind of trends before 1890 explaining for example the temperature decrease by the Tambora eruption in 1815. The temperature measurements starting from 1880 show almost as great differences as the proxy temperature graphs. The author has used the average of two different temperature measurement data sets published in 1975 [10] and the other in 1981 [12] for the period from 1889 to 1979. Because these data sets were published before the warming period since 1975, there has been no pressure to show any extra warming trend as it may now be a case. The author has used the UAH data set from 1980 onward. There was practically no difference between the temperature trends of UAH and GISS from 1979 to 2005 published before 2008 but thereafter the difference has increased to 0.26 ☐C arousing doubts about the accuracy of latest version of GISS-16.

Many research studies show that Pacific Decal Oscillation (PDO) phenomenon causes climate variations in the Pacific Basin and in the North America. The ENSO (El Nino-

Southern Oscillation) causes also very clear climate impacts. The Atlantic Multi-decadal Oscillation (AMO) correlates with the sea surface temperature of the North Atlantic Ocean. By analyzing the long-term PDO index and the AMO index, it can be found that they follow quite well the general temperature trend of the Earth. For example, the high temperature periods of 1930's and 2000's happen at the same time as the maximum values of PDO and AMO index. The author's conclusion is that the oscillation phenomena like PDO and AMO are not the real root causes of the long-term climate change but they have the common origin.

The warming impact of GH gases has increased from 0 % in 1750 to 37 % in 2015. The Astronomic Harmonic Resonances (AHR) can explain the temperature peaks of the 1930's and the present warming period since 2000. The change in Sun activity explains the low temperatures during the LIA. Therefore, these climate forces should be included into the overall climate model.

5. CONLUSIONS

The semi empirical climate model SECM has the coefficient of correlation $r^2 = 0.90$ and the standard error is 0.09 □C. The SECM follows the ups and downs of the T-comp very well. The TSI variation is the major driving force of the temperature increase having the contribution of 71-73 % during 19th and 20th centuries. Lean et al. [47] have carried out the correlation analysis between the NH surface temperature and the reconstructed solar irradiation and they found that a solar induced warming was 0.51 □C from the LIA in the 1990's and the correlation was 0.86. This result is in line with the results of this study but the overall accuracy of SECM in this study is better, because of GHG and AHR effects included.

The Anthropogenic Global Warming (AGW) theory cannot explain any periods with decreasing temperatures. It is also obvious that the climate model of IPCC [1], which is based on the sums of the radiative forcings (RF), gives about 50 % too high of a value in 2015. In this study, the author has used the formula of Ollila [22] in calculating the warming impact of CO_2. This formula does not assume the constant relative humidity but the constant absolute humidity both in the radiative forcing and in the climate sensitivity parameter calculations.

The four scenarios calculated to 2100 show that the temperature would start to decrease after 2020 even though the TSI level would stay at the present level.

6. COMPETING INTERESTS

The author declares that there are no competing interests existing.

REFERENCES

1. IPCC. The Physical Science Basis, Working Group I Contribution to the IPCC Fifth Assessment Report of the Intergovernmental Panel on Climate Change, Cambridge University Press, Cambridge, 2013.
2. Briffa KR, Osborn TJ, Schweingruber FH, et al. Low-frequency temperature variations from a northern tree ring density network, J Geophys Res 2001; 106: 2929–2941.
3. Moberg A, Sonechkin DM, Holmgren K, et al. Highly variable Northern Hemisphere temperatures reconstructed from low- and high-resolution proxy data. Nature 2005; 433: 613–617.

473   4. Lungqvist FC. A new reconstruction of temperature variability in the extra-tropical
474   Northern Hemisphere during the last two millennia. Geogr Ann 92 A 2010; 3: 339–351.
475   5. UAH. UAH MSU temperature dataset,
476   http://vortex.nsstc.uah.edu/data/msu/v6.0beta/tlt/uahncdc_lt_6.0beta5.txt (accessed 10
477   Dec 2016).
478   6. HadCRUT4. Temperature dataset, https://eosweb.larc.nasa.gov/project/erbe/erbe_table
479   41 (accessed 10 Dec 2016).
480   7. GISS. Temperature dataset,
481   http://data.giss.nasa.gov/gistemp/tabledata_v3/GLB.Ts+dSST.txt 42 (accessed 10 Dec
482   2016).
483   8. Peterson TC. Monitoring and understanding changes in heat waves, cold waves, floods,
484   and droughts in the United States. Am Met Sc 2013; June: 821-834.
485   9. Kelly M J. Trends in extreme weather events since 1900 – An enduring conundrum for
486   wise policy advice. J Geogr Nat Disast 2016; 155: 1-7, doi:10.4172/2167-0587.1000155.
487   10. National Academy of Sciences. Understanding climate change, a program for action.
488   United States Committee for the Global Atmospheric Research Program, Washington
489   D.C., 1975, p. 239.
490   11. Budyko MI. The effect of solar variations on the climate of the Earth. Tellus 1969; XXI:
491   611-619.
492   12. Hansen J, Johnson D, Lacis A, et al. Climate impact of increasing atmospheric carbon
493   dioxide. Science 1981; 213: 957-966.
494   13. Angell JK and Korshover J. Global temperature variation, surface – 100 mb: An update
495   into 1977. Mon Weather Rev 1978; 106 (6): 755-770.
496   14. Soon W, Connolly R and Connolly M. Re-evaluating the role of solar variability on
497   Northern Hemisphere temperature trends since the 19th century. Earth-Sci Rev 2015;
498   150: 409-452.
499   15. IPCC. Climate response to radiative forcing, IPCC Fourth Assessment Report (AR4), The
500   Physical Science Basis, Contribution of Working Group I to the Fourth Assessment
501   Report of the Intergovernmental Panel on Climate Change, Cambridge University Press,
502   Cambridge, 2007.
503   16. Myhre G, Highwood EJ, Shine KP, et al. New estimates of radiative forcing due to well
504   mixed greenhouse gases. Geophys Res Lett 1998; 25: 2715-2718.
505   17. Aldrin M, Holden M, Guttorp P, et al. Bayesian estimation on climate sensitivity based on
506   a simple climate model fitted to observations of hemispheric temperature and global
507   ocean heat content. Environmetrics 2013; 23: 253-271.
508   18. Bengtson L and Schwartz SE. Determination of a lower bound on earth's climate
509   sensitivity. Tellus 2013; B: 65, doi:http://dx.doi.org/10.3402/tellusb.v65i0.21533.
510   19. Otto A, Otto FEL, Allen MR, at al. Energy budget constraints on climate response. Nature
511   Geoscience 2016; 6: 415-416, http://dx.doi.org/10.1038/ngeo1836.
512   20. Lewis NJ. An objective Bayesian improved approach for applying optimal fingerprint
513   techniques to estimate climate sensitivity. J Clim 2013; 26: 7414-7429.
514   21. Harde H. Advanced two-layer climate model for the assessment of global warming by
515   CO_2. Open J Atm Clim Change 2014; 1: 1-50.
516   22. Ollila A. The potency of carbon dioxide (CO_2) as a greenhouse gas. Dev Earth Sci 2014;
517   2: 20-30.
518   23. Ollila A. Warming effect reanalysis of greenhouse gases and clouds. Ph Sc Int J 2017;
519   13: 1-13.
520   24. Ollila A. Cosmic theories and greenhouse gases as explanations of global warming. J
521   Earth Sci Geo Eng 2015; 5: 27-4.
522   25. Lean J. Solar Irradiance Reconstruction, IGBP PAGES/World Data Center for
523   Paleoclimatology Data Contribution Series # 2004-035, NOAA/NGDC Paleoclimatology
524   Program, Boulder CO, USA, 2004.

525   ftp://ftp.ncdc.noaa.gov/pub/data/paleo/climate_forcing/solar_variability/lean2000_irradianc
526   e.txt
527 26.Hoyt DV and Schatten KH. A discussion of plausible solar irradiance variations, 1700-
528   1992. J Geo Res 1993; 98: 18895-18906.
529 27.Bard E, Raisbeck G, Yiou F, et al. Solar irradiance during the last 1200 years based on
530   cosmogenic nuclides. TELLUS B 2000; 52: 985-992.
531 28.PMOD/WRC, Physikalisch-Meteorologisches Observatorium Davos. PMOD composite of
532   the solar constant. https://www.pmodwrc.ch/pmod.php?topic=tsi/composite/SolarConstant
533 29.Ollila A. Dynamics between clear, cloudy and all-sky conditions: cloud forcing effects. J
534   Chem Bio Phy Sci 2013; 4: 557-575.
535 30.McIntyre S and McKitrick R. Corrections to the Mann et al., (1998) proxy data base and
536   Northern Hemispheric average temperature series. Ener & Environ 2003; 14: 751– 771.
537 31.Alley RB. The Younger Dryas cold interval as viewed from central Greenland. Quaternary
538   Sc Rev 2000; 19: 213-226.
539 32.Esper J, Duthorn E, Krusic PL, et al. Nothern European summer temperature variations
540   over the Common Era from integrated tree-ring density records. J Quaternary Sc 2014;
541   29(5): 487-494.
542 33.Svensmark H. Influence of cosmic rays on earth's climate. Ph Rev Let 1998; 81: 5027-
543   5030.
544 34.Svensmark H, Bondo T and Svensmark J. Cosmic ray decreases affect atmospheric
545   aerosols and clouds. Geoph Res Lett 2009; 36: L15101, doi:10.1029/2009GL038429.
546 35.ISCCP. Radiation fluxes, http://isccp.giss.nasa.gov/products/products.html 39 (2016,
547   accessed 10 Dec 2016).
548 36.Kauppinen J, Heinonen JT and Malmi PJ. Major Portions in Climate Change: Physical
549   approach. Int Rev Phy 2011; 5: 260-270.
550 37.Scafetta N. Empirical evidence for a celestial origin of the climate oscillations and its
551   implications. J Atmos Sol-Terr Phy 2010; 72: 951-970.
552 38.Ermakov V, Okhlopkov V, Stozhkov Y, et al. Influence of cosmic rays and cosmic dust on
553   the atmosphere and Earth's climate. Bull Russ Acad Sc Ph 2009; 73: 434-436.
554 39.Gold T. Resonant orbits of grains and the formation of satellites. Icarus 1975; 25: 489-
555   491.
556 40.Wyatt MC, Dermott SF, Grogan K, et al. A unique view through the Earth's resonant ring,
557   Astrophysics with infrared surveys: A prelude to SIRTF, ASP Conference Series, 177, 1-
558   6, 1999.
559 41.Dermott SF, Jayaraman S, Xu Y-L, et al. A circumsolar ring of asteroidal dust in resonant
560   lock with the Earth. Nature 1994; 369: 719–723.
561 42.NASA. Jet Propulsion Laboratory: Horizons web-interface,
562   http://ssd.jpl.nasa.gov/horizons.cgi, (accessed 1 Dec 2016).
563 43.Wang J, Rossow WB and Zhang Y. Cloud vertical structure and its variations from a 20-yr
564   global rawinsonde dataset. J Climate 2016; 13: 3041-3056.
565 44.Bradley RS. The explosive volcanic eruption signal in northern hemisphere continental
566   temperature records. Climate Change1998; 12: 221-243.
567 45.Thomas M A. Simulation of the climate impact of Mt. Pinatubo eruption using ECHAM5.
568   PhD Thesis, Hamburg University, Germany, 2008.
569 46.Shepherd SJ, Zharkov SI and Zharkova VV. Prediction of solar activity from solar
570   background magnetic field variations in cycles 21-23. Astrophys J 2014; 795: 46,
571   doi:10.1088/0004-637X/795/1/46.
572 47.Lean J, Beer J and Bradley R. Reconstruction of solar irradiance since 1610: Implication
573   for climate. Geoph Res Lett 1995; 22(23): 3195-3198.
574